

Performance comparison between electromechanical and electro-hydrostatic regenerative shock absorbers

Original

Performance comparison between electromechanical and electro-hydrostatic regenerative shock absorbers / Galluzzi, R; Circosta, S; Amati, N; Tonoli, A. - In: IOP CONFERENCE SERIES: MATERIALS SCIENCE AND ENGINEERING. - ISSN 1757-8981. - 1214:1(2022), p. 012012. [10.1088/1757-899X/1214/1/012012]

Availability:

This version is available at: 11583/2952358 since: 2022-01-23T14:19:32Z

Publisher:

IOPscience

Published

DOI:10.1088/1757-899X/1214/1/012012

Terms of use:

This article is made available under terms and conditions as specified in the corresponding bibliographic description in the repository

Publisher copyright

(Article begins on next page)

PAPER • OPEN ACCESS

Performance comparison between electromechanical and electro-hydrostatic regenerative shock absorbers

To cite this article: R Galluzzi *et al* 2022 *IOP Conf. Ser.: Mater. Sci. Eng.* **1214** 012012

View the [article online](#) for updates and enhancements.

You may also like

- [\(Invited\) Dry Electrode Process Technology](#)
Hieu Duong, Arek Suszko and Haim Feigenbaum
- [\(Invited\) Beyond-CMOS Device and Interconnect Technology Benchmarking Based on a Fast Cross-Layer Optimization Methodology](#)
Chenyun Pan and Azad Naeemi
- [Modeling Water Management and Carbon Dioxide Contamination Effects in Anion-Exchange Membrane Fuel Cells](#)
Michael R. Gerhardt, Lalit M. Pant and Adam Z. Weber



The Electrochemical Society
Advancing solid state & electrochemical science & technology

242nd ECS Meeting

Oct 9 – 13, 2022 • Atlanta, GA, US

Abstract submission deadline: **April 8, 2022**

Connect. Engage. Champion. Empower. Accelerate.

MOVE SCIENCE FORWARD



Submit your abstract



Performance comparison between electromechanical and electro-hydrostatic regenerative shock absorbers

R Galluzzi¹, S Circosta², N Amati² and A Tonoli²

¹ School of Engineering and Sciences, Tecnológico de Monterrey, Mexico City 14380, Mexico

² Department of Mechanical and Aerospace Engineering, Center for Automotive Research and Sustainable Mobility@PoliTO, Politecnico di Torino, 10129 Turin, Italy

E-mail: renato.galluzzi@tec.mx

Abstract. Controllable damping solutions are increasingly finding their way into passenger cars and other vehicles. They improve ride quality by enhancing comfort and handling performance. Semi-active solutions based on controlled valves or variable-rheology fluids are by far the most common technologies in the automotive industry. However, regenerative alternatives that employ electric machines can be seen as a desirable evolution of the suspension market. In this context, the present paper studies two regenerative solutions: electro-hydrostatic and rotary electromechanical dampers. Transmission interfaces are particularly relevant in these technologies. Adequate choices are needed to guarantee proper packaging, performance, structural integrity, and high efficiency. This work compares both technologies in terms of design and packaging. Furthermore, experimental results are analysed to understand the performance of damping solutions. It is demonstrated that the rotary electromechanical device outperforms its electro-hydrostatic counterpart in important features, such as conversion efficiency, envelope, mass and dynamic behaviour.

1. Introduction

Current trends in the automotive field foresee a strong push towards the electrification of power-train and chassis devices. This change has been driven by the search of more sustainable energies, and the inclusion of smart features. The so-called *x-by-wire* technologies are finding their implementation through the addition of numerous mechatronic solutions.

In ground vehicles, smart actuators have been proposed to control different parameters of the vehicle suspension. Since the seminal work proposed by Karnopp [1], damping has been regulated predominantly through semi-active means using solenoid valves or fluid rheology, thus allowing comfort or handling enhancement. However, recent efforts have proposed the use of electromagnetic damping solutions. They exploit an electric machine—linear or rotary—to control suspension forces. From an energy standpoint, actuators of this type are intrinsically bidirectional. This means that electric machines can absorb or exert power. Hence, they provide active or damping forces to the suspension. Furthermore, when damping, they offer regenerative capability, i.e. vibrational energy can be partially transformed into electricity. Active suspensions are particularly attractive for the autonomous vehicle paradigm, as they provide improved vibration suppression for the chassis, so passengers can focus on secondary activities comfortably while travelling.

The aforementioned benefits have led to numerous research efforts in the field of regenerative damping solutions [2]. The use of electric machines brings the benefit of linearity, simple, well-known dynamics and improved controllability with respect to other technologies. However, a key challenge of



Content from this work may be used under the terms of the [Creative Commons Attribution 3.0 licence](https://creativecommons.org/licenses/by/3.0/). Any further distribution of this work must maintain attribution to the author(s) and the title of the work, journal citation and DOI.

regenerative solution consists in identifying and implementing a proper transmission system to interface the electric machine with the vehicle suspension.

Although linear motors [3] fit well with the natural stroke of conventional shock absorbers, their limited force-to-mass ratio makes them unsuitable for many vehicles. Thereby, linear-to-rotary conversion is needed. In this regard, numerous attempts have been made with different mechanisms: ball screw [4, 5], rack-pinion [6] and rotary with lever [7, 8, 9]. In an attempt to inherit the use of fluid from passive solutions, electro-hydrostatic actuators with hydraulic pistons and fixed-displacement pumps have been also proposed for this task [10, 11].

Despite the numerous efforts, there is no clear indication as to which trend to follow: electro-hydrostatic or electromechanical. Comparison attempts have been carried out to identify the most suitable technology. However, many of these technologies are developed *ad hoc* for specific applications, thus hindering direct, one-to-one technology comparisons.

To address this shortcoming, the present paper provides two detailed design alternatives for specific regenerative suspension requirements. Specifically, electro-hydrostatic (EHA) and rotary electromechanical (REM) versions of a regenerative shock absorber are designed, built and tested. Design aspects for each technology have been already discussed in previous works [7, 10]. Nevertheless, the aim of this paper is to present them in a comparative manner in terms of design choices, prototype features and their experimental response.

This work is organised as follows. Section 2 describes the damping requirements. Subsequently, section 3 outlines the design for the offered damping solutions to reach the final layout of both actuators. Then, section 4 presents experimental results. In section 5, solutions are compared. Finally, section 6 concludes the work.

2. Requirements

For the present comparative analysis, a B-class vehicle is taken as a reference. In the suspension, a maximum-damping piecewise characteristic is desirable (see figure 1). Thus, a first damping coefficient $c_1 = 10 \text{ kNs/m}$ is needed within damping speeds $|v_d| \leq 0.1 \text{ m/s}$. Above 0.1 m/s , significantly lower coefficients are expected: $c_2 = 0.5 \text{ kNs/m}$. Besides damping, maximum damping force ($F_{d,max} = 2 \text{ kN}$) and speed ($v_{d,max} = 2 \text{ m/s}$) are relevant design specifications.

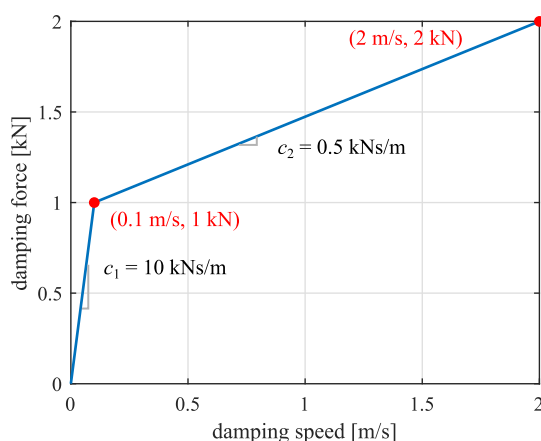


Figure 1. Target maximum damping specification.

Although the damping characteristic already highlights important design parameters, simulations are needed to understand the expected duty cycle of the shock absorber. This is particularly relevant to size the electric machine in regenerative solutions. To this end, vertical dynamics can be analysed through a quarter-car model (figure 2).

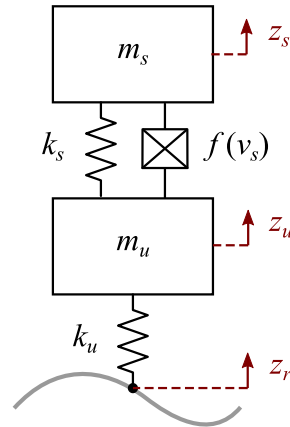


Figure 2. Quarter-car model to evaluate damper duty cycle.

The chassis of the vehicle (sprung mass m_s) is connected to the wheel hub (unsprung mass m_u) by means of a suspension spring (stiffness k_s) and shock absorber (piecewise damping $f(v_d)$). In turn the wheel hub receives the road unevenness vibrations through the tyre (stiffness k_u).

To reproduce realistic damping load profiles, the model in figure 2 must be simulated with the damping characteristic curve presented in figure 1 and a realistic road profile for $z_r(t)$. These conditions lead to a root-mean-square (RMS) damping force $F_{d,rms} \cong 504 \text{ N}$ when the parameters in table 1 are used.

Table 1. Quarter-car model parameters.

Description	Symbol	Value	Unit
Sprung mass	m_s	417	kg
Unsprung mass	m_u	40	kg
Suspension stiffness	k_s	23	kN/m
Tyre stiffness	k_u	226	kN/m
Vehicle cruise speed	v_{car}	70	km/h
Road roughness index (B class, ISO 8608)	G_r	$6.4 \cdot 10^{-7}$	$\text{m} \cdot \text{cycle}$

3. Design

3.1. Overview

The aim of the design is to size the transmission and the electric machine of the actuator. The transformation from the rotary domain to the linear one is obtained by means of the transmission ratio τ_t [m/rad]. In an EHA solution, this relation is ideally attained by closing a hydrostatic circuit with a pump unit (fixed displacement D_p) and a hydraulic cylinder (piston cross section A_p), thus

$$\tau_t = \frac{D_p}{A_p} \quad (1)$$

Likewise, for a REM solution, this transformation is achieved through a linkage with transmission ratio τ_l [m/rad]. Usually, an additional gearbox multiplier (τ_g) is required to achieve the target

performance:

$$\tau_t \cong \tau_l \tau_g \quad (2)$$

Disregarding the type of actuator, the definition of the transmission ratio allows designing the electric machine. From a practical standpoint, a feasible transmission system able to guarantee τ_t is needed. This process is usually iterative, as a high degree of integration among subsystems is desirable.

3.2. Electric machine

The design of the electric machine must maximise the machine output torque (T_m), while satisfying working and geometric constraints. To simplify this step, a candidate machine can be designed either by analytic means or through the finite-element method. To match a desired envelope for the actuator, the stator outside radius r_{so} must be constrained. A design procedure in two dimensions yields the torque per unit length r_{Tl} [Nm/m]. Subsequently, the machine active length l_a can be adjusted to match the desired output torque.

The design of electric machinery is a research area *per se* and thus, is not covered thoroughly in this work. Nevertheless, some considerations can be followed for compact actuators. In particular, a three-phase permanent-magnet brushless machine is proposed to maximise torque density. Concentrated winding solutions are preferred due to their lower Joule losses, shorter end turns and simpler winding layouts. For the target machine size, a configuration with 12 slots and 10 magnets is selected. The machine geometry is optimised to yield maximum torque while avoiding saturations on the magnetic circuit. The obtained machine design is shown in figure 3 and its parameters are listed in table 2.

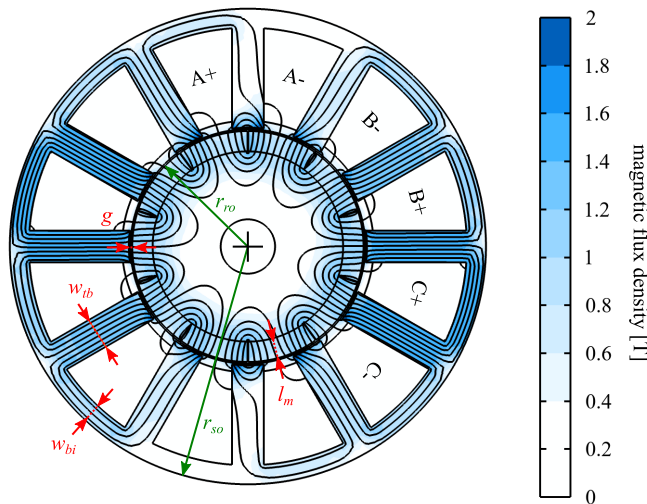


Figure 3. Electric machine cross section. The colour map indicates the flux density norm distribution, whereas the contour lines denote the out-of-plane magnetic vector potential. Letters in the slots indicate the winding layout for the three phases (A,B,C). Dimensions are reported in table 2.

Once that the machine has been designed in two dimensions, an effective approach should size the transmission ratio and the output torque of the machine, given that, in static conditions

$$F_d = \frac{T_m}{\tau_t} \quad (3)$$

$$\omega_m = \frac{v_d}{\tau_t} \quad (4)$$

Table 2. Electric machine parameters.

Description	Symbol	Value	Unit
Phase resistance	R	20	m Ω
Inductance (d and q axes)	L_{dq}	80	μ H
Phase back-EMF constant	K_e	23	mVs/rad
Nominal torque	T_n	0.7	Nm
Maximum torque	T_{max}	2.3	Nm
DC link voltage	V_{dc}	48	V
Base speed	ω_n	10	krpm
Maximum generator efficiency	η_g	0.88	–
Stator outside radius	r_{so}	35	mm
Rotor outside radius	r_{ro}	14	mm
Stator back iron width	w_{bi}	2.8	mm
Stator tooth base width	w_{tb}	4.7	mm
Air gap	g	0.5	mm
Permanent magnet length	l_m	3	mm
Active length	l_a	22	mm

Thus, assuming constant electric machine torque, the damping force can be maximised by reducing τ_t as much as possible. However, this poses a bi-fold effect, as it would lead to very high angular speed (ω_m) given a fixed damping speed. Moreover, in linear-to-rotary transmissions, the inertia of rotating parts J_m and viscous damping c_m are transported to the linear domain as

$$c_{eq} = \frac{c_m}{\tau_t^2} \quad (5)$$

$$m_{eq} = \frac{J_m}{\tau_t^2} \quad (6)$$

These equivalent parameters exhibit a quadratic inverse relation with the transmission ratio.

A proper selection of τ_t and l_a depends on specific criteria, as listed below.

3.2.1. Continuous operation. For machines cooled by natural air convection, continuous operation is attained with an RMS wire current density of 6 A/mm² [12]. In this case, the motor should be able to guarantee the RMS damping force obtained from the simulations in section 2 ($F_{d,rms} \cong 504$ N):

$$F_{d,rms} = \frac{T_{m,cont}}{\tau_t} = r_{Tl,cont} \frac{l_a}{\tau_t} \quad (7)$$

3.2.2. Impulsive operation. In transient conditions, air-cooled machines can attain 20 A/mm² of current density for few seconds. The machine should comply with maximum force requirements in this condition ($F_{d,max} = 2$ kN):

$$F_{d,max} = \frac{T_{m,max}}{\tau_t} = r_{Tl,max} \frac{l_a}{\tau_t} \quad (8)$$

3.2.3. Damping coefficient. For electromagnetic devices, the maximum viscous damping is attained in short circuit and it is inversely proportional to the phase resistance:

$$c_{eq,max} = \frac{3K_e^2}{2\tau_t^2 R} \quad (9)$$

where K_e is the motor back-electromotive force (EMF) constant and the phase resistance is given by

$$R \cong \frac{2N_c N_t \rho_{Cu} l_a}{A_w} \quad (10)$$

being N_c the number of series coils per phase, N_t the number of turns per coil, A_w the wire cross section and ρ_{Cu} the resistivity of copper.

The combination of the most conservative force constraint (equation 7 or 8) with the maximum damping requirement (expressions 9 and 10) lead to an optimal choice of motor active length l_a and total transmission ratio τ_t . For the present study, a transmission ratio $\tau_t = 1.3$ mm/rad and an active length $l_a = 22$ mm are determined.

3.3. Motion transmission

Up to this point, both solutions share the same electric machine and total transmission ratio. However, there are significant differences regarding how τ_t is achieved.

3.3.1. Electro-hydrostatic transmission. This transmission is achieved by coupling a hydraulic cylinder with a pump. To reuse the passive shock absorber tube and piston, a cross section $A_p = 4.2$ cm² is preserved. According to equation 1, a fixed volumetric displacement $D_p = 3.6$ cm³/rev is required to match the target transmission ratio.

To favour low friction and extended lifespan, gerotor pump is selected for the task. A seven-chamber device is designed with trochoidal gear profiles and maximum eccentricity to minimise its envelope. With a pressure range up to 60 bar, gerotor clearances are tuned to fulfil a suitable trade-off between leakages and mechanical losses [13]:

- Total axial clearance: 20 μ m
- Outer gear outside diameter clearance: 80 μ m
- Inner gear inside diameter clearance: 20 μ m
- Tooth tip clearance: 40 μ m

The EHA solution depicted in figure 4 packs a motor (4,7) and a pump (1,2) within the same pressure-tight oil medium. The inner gear (1) of the pump is directly coupled to the electric motor shaft (10). The outer gear (2) is supported hydrostatically by a journal bearing machined on the casing (9). The rotor of the unit is supported by two ball bearings (3) in a face-to-face arrangement. The unit is coupled to the chambers of the damper by means of a hydraulic manifold (11) welded onto the shock absorber tube. The rotor position is measured by means of a Hall sensor array (7) that measures the magnetic field of permanent magnets on one end of the rotor shaft. The back of the motor cover (8) presents four sealing cable glands (5) that are used to access power and signal wirings. A drain cap (6) is used to ease oil filling.

3.3.2. Lever and multiplier transmission. In this case, the total transmission ratio τ_t is split between a linkage (τ_l) and a gearbox multiplier (τ_g). Since the lever system is mainly conceived for new suspension architectures, it is defined in an initial step. In the present study, we refer to a four-bar kinematic assembly in which the end rod is fixed onto the passive shock absorber tube. The latter is preserved for structural

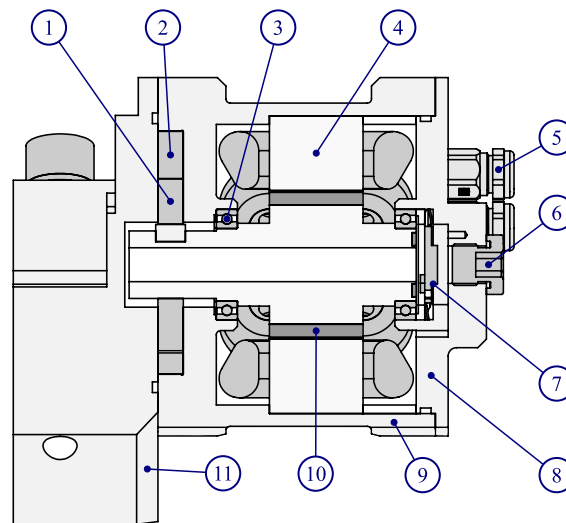


Figure 4. Electro-hydrostatic damper actuation unit. (1) gerotor inner gear; (2) gerotor outer gear; (3) motor ball bearing [$\times 2$]; (4) stator assembly; (5) cable gland [$\times 4$]; (6) drain cap; (7) position sensor; (8) motor cover; (9) casing; (10) rotor assembly; (11) manifold.

purposes only. In the future, the shock absorber tube will be removed and the rod end will be connected to other suspension parts. In this layout, a linkage with $\tau_l = 115 \text{ mm/rad}$ is obtained.

To fulfil $\tau_t = 1.3 \text{ mm/rad}$, a two-stage planetary multiplier is designed. Each stage presents a ratio of $1/9.375$, thus leading to a total ratio of $\tau_g = 1/87.89$. Gear profiles are carefully defined to match load and fatigue considerations from the ISO 6336 method B standards.

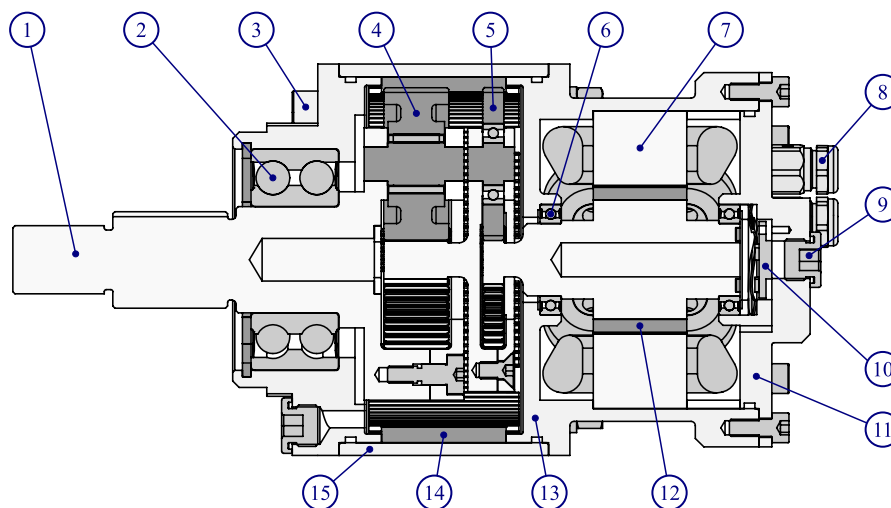


Figure 5. Rotary electromechanical damper actuation unit. (1) input shaft; (2) input bearing; (3) gearbox cover; (4) first stage assembly; (5) second stage assembly; (6) motor ball bearing [$\times 2$]; (7) stator assembly; (8) cable gland [$\times 4$]; (9) drain cap [$\times 2$]; (10) position sensor; (11) motor cover; (12) rotor assembly; (13) motor casing; (14) outer ring gear; (15) gearbox casing.

The final assembly embodies the same electric machine (7,12) as the EHA counterpart. In contrast, the rotor tip presents a sun gear profile that interfaces directly to the second stage (5) of the multiplier (2). An input splined shaft (1) is connected to the linkage. Axial and radial forces are supported by a

double-row angular contact ball bearing arrangement (2). The same input shaft serves as a carrier of the first stage (4). An outer ring gear (14) is shared by both stages in a gearbox casing (15). Gearbox components are axially constrained by a gearbox cover (3) and a motor casing (13). As the EHA unit, the motor side presents a motor cover (11), a feedback sensor (10), ball bearings for the rotor shaft (6) and cable glands (8). Drain caps (9) help in this case to introduce gearbox lubricants.

Final versions of both prototypes are shown in figures 6 and 7.

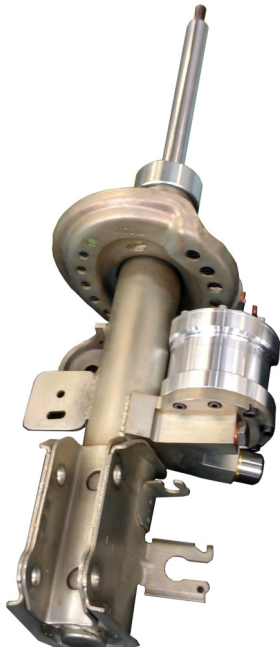


Figure 6. Picture of the electro-hydrostatic damper prototype installed on a shock absorber.

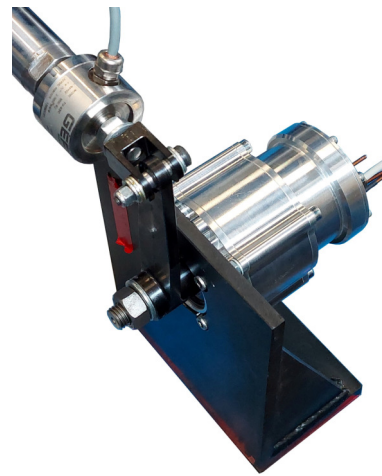


Figure 7. Picture of the rotary electromechanical damper prototype with its linkage.

4. Experimental characterisation

The goal of the experimental characterisation is to understand the power contributions involved in multiple operating points and define the efficiency behaviour of the regenerative damper prototypes. This allows for a proper comparison of both technologies.

4.1. Test procedure

During testing, prototype inputs must be driven by means of a physical flow variable, while they impose a damping torque. To this end, their electric machine is current-controlled with field-oriented techniques using custom power and logic hardware. Specifically, the motors are characterised in the regenerative (damping) quadrant with a quadrature current ramp profile $I_q(t)$ increasing from zero to 25 A at a rate of 1 A/s. This profile allows spanning multiple operating points in regeneration.

To drive the EHA unit, an additional motor (Kollmorgen™ DBL5) and a pump (Parker™ MGG2) are directly coupled to the prototype pump by means of a manifold and two circuit lines, as seen in figure 8. The driving motor imposes steady angular speed ω_d , which in turn becomes a constant flow rate on the hydraulic ports of the characterised device through the driving pump (fixed displacement of 11.43 cm³/rev). During testing, the hydraulic power is calculated by means of the pressure drop Δp_h measured by two GEFTRAN™ TK sensors, and flow rate Q_h sensed by a KEM™ HM11 meter. The

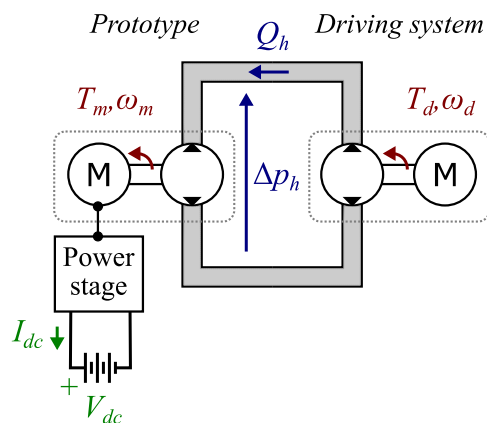


Figure 8. Scheme of the electro-hydrostatic damper prototype test bed.

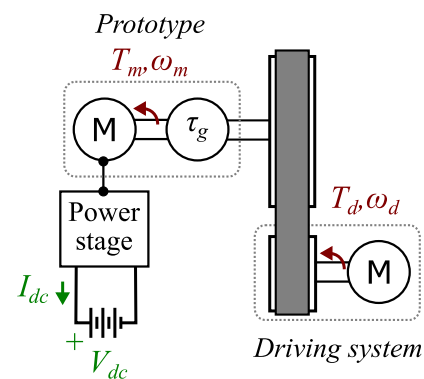


Figure 9. Scheme of the rotary electromechanical damper prototype test bed.

mechanical power is obtained from the prototype speed feedback (ω_m) and the torque estimated from the current ($T_m \cong 3K_e I_q/2$). Finally, the regenerated power is obtained from the DC link battery voltage (V_{dc}) and current (I_{dc}) signals.

Similarly, the REM unit is tested by means of the belt-pulley system schematised in figure 9. The transmission is driven by an electric machine (Kollmorgen™ DBL5), which again imposes constant angular speed ω_d through a pulley ratio of 2. The input mechanical power is obtained from the driving motor torque (T_d) and speed (ω_d), while the regenerated power is measured from DC link variables.

In both test setups, signals were synchronously acquired using an LMS™ SCADAS system at a sample rate of 12.8 kHz.

4.2. Results

Power contributions and conversion efficiency results are reported in figures 10 and 11 for EHA and REM prototypes, respectively. In both cases, results are reported for different constant speeds of the driving unit.

Both prototypes were able to span a significant portion of the force-speed plane. The EHA unit could range from 300 to 1.4 kN; these forces were calculated as $F_d = \Delta p_h A_p$. The REM solution yielded lower forces between 110 and 876 N. This difference can be attributed to constructive features of the two test beds, which fundamentally operate under diverse physical principles. More importantly, the EHA solution showed larger friction losses, thus limiting the minimum attainable force, even in the absence of electromagnetic damping. To confirm this point, figure 12 depicts the characterised points in the force-speed plane, where the target maximum damping curve is reported for comparison purposes.

A further difference is seen in the entity of power contributions. The REM device presents a mechanical input power and an output electrical power at the DC link. Conversely, the EHA device shows an additional hydraulic power term. While mechanical power usually increases the effort output due to friction, hydraulic power involves flow losses. In other words, an EHA solution presents leakages that eventually reduce the motion transmission. By comparing the hydraulic and mechanical power terms of the EHA device, one can observe a net decrease in the latter at high forces. In fact, high forces imply larger pressure drops, which in turn amplify leakages in the pump gaps. These phenomena are also present in the gaps between the piston and the damper tube, but these components did not take part of the experimental campaign. In turn, power terms from the REM solution show steadier behaviour due to an ideally rigid motion ratio without flow (speed) reduction. Leakage losses are also advisable in figure 12, where the effective damping speed of the EHA device decreases as force ramps up.

The presence of multiple conversion stages hinders the EHA device total conversion efficiency,

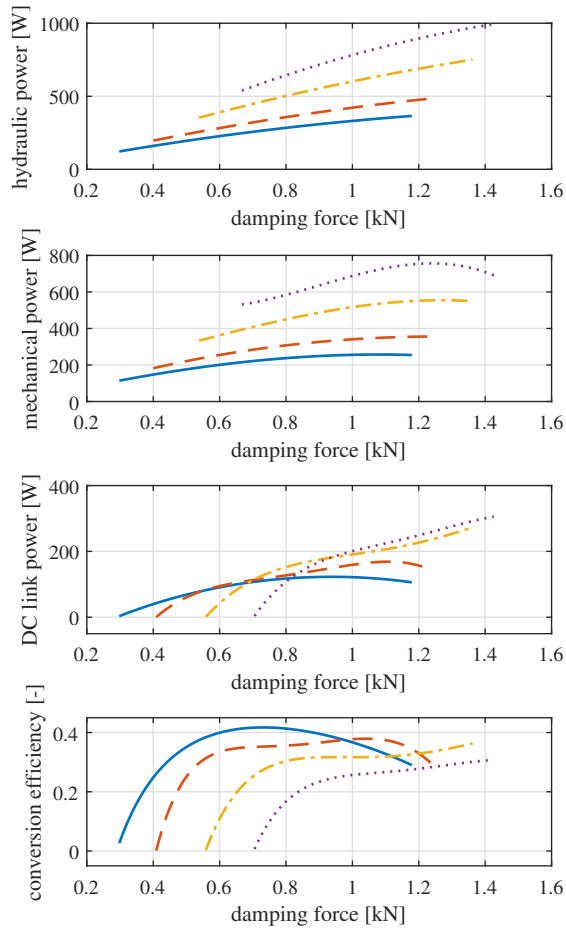


Figure 10. Electro-hydrostatic damper prototype test results. Power contributions and conversion efficiency at constant speed of the driving motor and pump: 1 (solid), 1.2 (dashed), 1.6 (dash-dotted) and 2krpm (dotted).

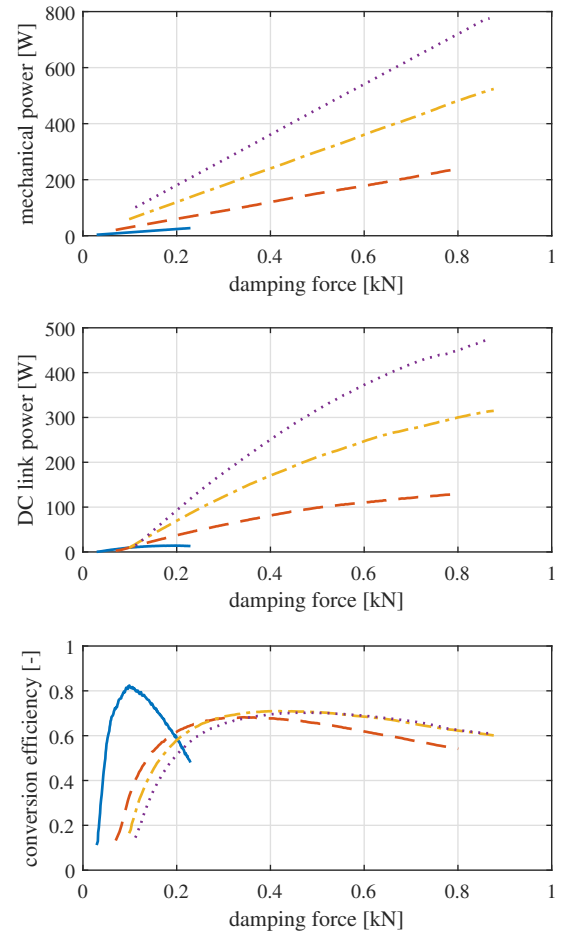


Figure 11. Rotary electromechanical damper prototype test results. Power contributions and conversion efficiency at constant speed of the prototype input shaft: 10 (solid), 25 (dashed), 50 (dash-dotted) and 75 rpm (dotted).

calculated as

$$\eta_{tot} = \frac{V_{dc}I_{dc}}{\Delta p_h Q_h} \quad (11)$$

which in the tests involving the lowest driving speed, led to a maximum of 0.417. At higher-valued inputs, the efficiency drops below 0.36 and presents a decreasing value as pressure escalates due to leakage effects.

By converse, the REM prototype shows more favourable results in this regard. With

$$\eta_{tot} = \frac{V_{dc}I_{dc}}{T_d \omega_d} \quad (12)$$

a maximum is found at 0.823, where the driving speed is the lowest setting (20 rpm on the driving motor, 10 rpm on the prototype input shaft). Higher speeds induce larger damping forces, but in this case, the efficiency finds maximum values close to 0.7, with very slight decays as force increases.

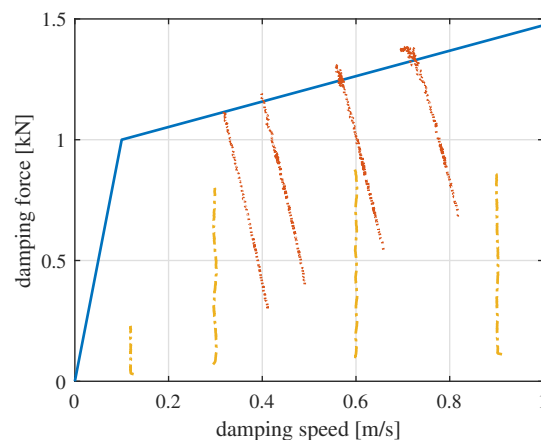


Figure 12. Characterised points in the force-speed plane for the electro-hydrostatic (dotted) and the rotary electromechanical (dash-dotted) prototypes. The target maximum damping characteristic (solid) is shown for comparison purposes.

5. Discussion

In the following, key features for both prototypes are compared. Table 3 summarises the comparison in qualitative terms. However, for some of the listed features, quantification is possible.

Table 3. Qualitative comparison among regenerative damper technologies.

Feature	Electro-hydrostatic	Rotary electromechanical
Mechanical robustness and fatigue	●	◐
Noise	◐	○
Oil-free	○	●
Conversion efficiency	◐	●
Packaging	◐	●
Actuator mass	◐	●
Equivalent inertia	◐	●
Total score units	●●●◐	●●●●●◐

Regarding mechanical robustness and fatigue, the EHA solution presents an advantage due to the intrinsic lubrication of the rotating parts, thus reducing tribology issues. Furthermore, gerotor pumps are well-known for inducing very low relative angular speeds among the parts in contact. The REM prototype, on the other hand, is lubricated with transmission oil, but the amount of parts in contact is much larger than in the EHA counterpart. In terms of noise, the presence of fluid dampens sound pressure emissions for the EHA solution. This is still applicable but less evident for the REM alternative.

The fluid presence becomes a downside when ageing, leakages and fluid contamination are accounted for. For this reason, many hydraulic devices in the automotive industry are being dismissed in favour of oil-free alternatives.

The conversion efficiency was demonstrated to be much lower and presented a narrow region for the EHA damper. This aspect is dominated by larger friction due to tight clearances between the gerotor gears and the pump casing. If clearances are increased to reduce friction, leakages would dominate significantly the behaviour.

When considering only the actuation units, the EHA device presents a maximum diameter of 88 mm and an axial length of 117 mm. The REM device is larger at 93 mm of diameter and 194 mm of axial length considering its input shaft. The mass of the REM prototype with linkage bars is 3.5 kg, while the EHA device and the shock absorber weigh 5.5 kg. Nevertheless, the use of a rotary electromechanical system could imply a total rethinking of the vehicle suspension with collateral benefits on the geometric envelope and distribution of masses. In addition, the REM prototype mass is added to the sprung component of the quarter-car model. The EHA, by converse, sits on the unsprung mass, thus having a more significant impact on vertical dynamics.

In terms of dynamic behaviour, the EHA system presents an equivalent inertia of 23 kg (equation 6). The REM device presents a lower inertial contribution of 15.9 kg. Despite sharing the same electric machine and overall transmission ratio, the moment of inertia of both gerotor gears is larger than that of rotating carriers and planets inside the gearbox. This inertial term is relevant as frequency escalates, as it tends to lock the suspension and eventually requires an active attenuation using the control system.

6. Conclusions

The present paper dealt with the comparison of electro-hydrostatic and rotary electromechanical regenerative damping technologies. A unified design for the electric machine and transmission ratio was motivated. Then, two different approaches led to the definition of specific transmission systems for both technologies. Details regarding packaging and assembly were discussed. The resulting prototypes were built and tested using dedicated test beds. Despite having different architectures, a similar testing methodology led to comparable results in terms of power contributions and conversion efficiencies. Finally, a discussion on qualitative and quantitative features of both technologies was carried out.

From the obtained results, it is clear that the rotary electromechanical solution outperforms the electro-hydrostatic one in terms of key metrics. However, the implementation of a rotary electromechanical damper requires important efforts to integrate the actuator into a conventional suspension, while electro-hydrostatic actuators fit in traditional layouts.

References

- [1] Karnopp D, Crosby M J and Harwood R A 1974 *Journal of Engineering for Industry* **96** 619–626
- [2] Abdelkareem M A A, Xu L, Ali M K A, Elagouz A, Mi J, Guo S, Liu Y and Zuo L 2018 *Applied Energy* **229** 672–699
- [3] Gysen B, Paulides J, Janssen J and Lomonova E 2010 *IEEE Transactions on Vehicular Technology* **59** 1156–1163
- [4] Tonoli A, Amati N, Detoni J G, Galluzzi R and Gasparin E 2013 *Vehicle System Dynamics* **51** 1186–1199
- [5] Kawamoto Y, Suda Y, Inoue H and Kondo T 2008 *Vehicle System Dynamics* **46** 1053–1063
- [6] Li Z, Zuo L, Kuang J and Luhrs G 2013 *Smart Materials and Structures* **22** 025008
- [7] Galluzzi R, Circosta S, Amati N and Tonoli A 2021 *Mechatronics* **77** 102580
- [8] Todmal P E and Melzi S 2020 *SAE International Journal of Passenger Cars - Mechanical Systems* **13** 06–13–01–0002
- [9] Yu M, Dini D and Cleaver G D 2018 *IEEE/ASME Transactions on Mechatronics* **23** 2066–2077
- [10] Galluzzi R, Xu Y, Amati N and Tonoli A 2018 *Applied Energy* **210** 16–27
- [11] Guo S, Xu L, Liu Y, Guo X and Zuo L 2017 *IEEE/ASME Transactions on Mechatronics* **22** 2684–2694
- [12] Dorrell D G, Hsieh M F, Popescu M, Evans L, Staton D A and Grout V 2011 *IEEE Transactions on Industrial Electronics* **58** 3741–3757
- [13] Tessari F, Galluzzi R and Amati N 2020 *Journal of Mechanical Design* **142** 063501